HAL
open science

Enhanced thermal sensitivity of MEMS bolometers integrated with nanometer- scale hole array structures

Ya Zhang, Boqi Qiu, Naomi Nagai, Masahiro Nomura, Sebastian Volz, Kazuhiko Hirakawa

To cite this version:

Ya Zhang, Boqi Qiu, Naomi Nagai, Masahiro Nomura, Sebastian Volz, et al.. Enhanced thermal sensitivity of MEMS bolometers integrated with nanometer- scale hole array structures. AIP Advances, 2019, 10.1063/1.5113521 . hal-02364483

HAL Id: hal-02364483

https://hal.science/hal-02364483

Submitted on 15 Nov 2019

HAL is a multi-disciplinary open access archive for the deposit and dissemination of scientific research documents, whether they are published or not. The documents may come from teaching and research institutions in France or abroad, or from public or private research centers.

L'archive ouverte pluridisciplinaire **HAL**, est destinée au dépôt et à la diffusion de documents scientifiques de niveau recherche, publiés ou non, émanant des établissements d'enseignement et de recherche français ou étrangers, des laboratoires publics ou privés.

AIP Advances

Enhanced thermal sensitivity of MEMS bolometers integrated with nanometer-scale hole array structures

Cite as: AIP Advances **9**, 085102 (2019); https://doi.org/10.1063/1.5113521
Submitted: 04 June 2019 . Accepted: 23 July 2019 . Published Online: 02 August 2019

Ya Zhang, Boqi Qiu, Naomi Nagai, Masahiro Nomura, Sebastian Volz, and Kazuhiko Hirakawa

View Online Export Citation CrossMark

ARTICLES YOU MAY BE INTERESTED IN

A generalized self-consistent model for quantum tunneling current in dissimilar metal-insulator-metal junction
AIP Advances **9**, 085302 (2019); https://doi.org/10.1063/1.5116204

Study on impulse quenching based multichamber arc quenching structure
AIP Advances **9**, 085104 (2019); https://doi.org/10.1063/1.5113853

Dependence of plasma current on object condition in atmospheric pressure non-thermal equilibrium argon plasma
AIP Advances **9**, 085202 (2019); https://doi.org/10.1063/1.5116268

© 2019 Author(s).

Enhanced thermal sensitivity of MEMS bolometers integrated with nanometer-scale hole array structures

Cite as: AIP Advances 9, 085102 (2019); doi: 10.1063/1.5113521
Submitted: 4 June 2019 • Accepted: 23 July 2019 •
Published Online: 2 August 2019

View Online Export Citation CrossMark

Ya Zhang,[1,2,a)] Boqi Qiu,[1] Naomi Nagai,[1] Masahiro Nomura,[1,3,4] Sebastian Volz,[4] and Kazuhiko Hirakawa[1,3,4,b)]

AFFILIATIONS

[1] Institute of Industrial Science, University of Tokyo, 4-6-1 Komaba, Meguro-ku, Tokyo 153-8505, Japan
[2] Institute of Engineering, Tokyo University of Agriculture and Technology, Koganei, Tokyo, 184-8588, Japan
[3] Institute for Nano Quantum Information Electronics, University of Tokyo, 4-6-1 Komaba, Meguro-ku, Tokyo 153-8505, Japan
[4] LIMMS/CNRS-IIS, UMI 2820, 4-6-1 Komaba, Meguro-ku, Tokyo 153-8505, Japan

[a)] **Electronic mail:** zhangya@go.tuat.ac.jp
[b)] **Electronic mail:** hirakawa@iis.u-tokyo.ac.jp

ABSTRACT

We have fabricated two-dimensional nanometer-scale hole array structures on GaAs doubly-clamped microelectromechanical system (MEMS) beam resonators to modulate their thermal properties. Owing to the reduction in the thermal conductance of the MEMS beams by introducing the hole array structures, the nano-porous MEMS bolometers show 2-3 times larger thermal sensitivities than the unpatterned reference sample. Furthermore, since the heat capacitance of the MEMS beams is also reduced by introducing the hole array, the thermal decay time of the patterned MEMS beams is increased only by about 30-50%, demonstrating the effectiveness of the hole array structures for enhancing the thermal sensitivities of bolometers without significantly deteriorating their operation bandwidths.

© 2019 Author(s). All article content, except where otherwise noted, is licensed under a Creative Commons Attribution (CC BY) license (http://creativecommons.org/licenses/by/4.0/). https://doi.org/10.1063/1.5113521

Micro-electromechanical system (MEMS) resonators[1–3] are very attractive for sensing applications. Owing to their high quality (Q)-factors, the MEMS resonators can detect a small change in the resonance frequencies and can be used to detect changes in mass,[4–8] charge,[9,10] spin orientation,[11,12] and temperature.[13,14] Recently, we have developed an uncooled, sensitive and fast bolometer by using a doubly clamped GaAs MEMS beam resonator for terahertz (THz) sensing applications.[15–17] The MEMS resonator detects THz radiation by measuring the shift in the resonance frequency caused by heating of the MEMS beam.[15–17] Since the responsivity of the MEMS resonators is inversely proportional to the thermal conductance of the MEMS beam, G_T, it is preferable to decrease G_T for enhancing the responsivity. On the other hand, the thermal time constant τ_D (= C_T/G_T; C_T is the heat capacitance of the MEMS beam) increases when G_T is decreased, leading to the reduction in the detection speed. This trade-off between the responsivity and the detection bandwidth exists in all kinds of thermal sensors.

Nano-porous structures such as slabs with one-dimensional (1D)[18] or two-dimensional (2D)[19–21] hole arrays have been proposed to engineer the thermal properties of materials. The hole array structures are promising for improving thermal responsivities of the MEMS resonators; the hole array structure can reduce the thermal conductance, G_T, of the MEMS beam by decreasing the cross section of the beam. Furthermore, the hole array structure reduces the heat capacitance of the beam, C_T, by decreasing the material volume. Therefore, the increase in τ_D due to the decrease in G_T is partly compensated by the reduction in C_T and it is possible to enhance the thermal responsivity, while keeping a fast detection speed of the MEMS thermal sensors.

In this work, we have fabricated 2D nanometer-scale hole array structures on the MEMS beam resonators to modulate their thermal

© Author(s) 2019

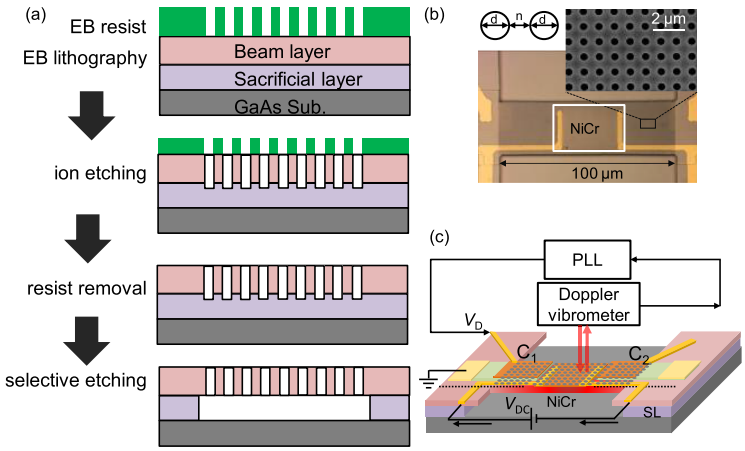

FIG. 1. (a) Fabrication processes of a MEMS resonator with a hole array structure. (b) Microscope image of a fabricated GaAs MEMS beam resonator (100×30×0.6 μm^3) with a 2D hole array structure of a hole diameter d = 500 nm and a neck size n = 500 nm. The Si-doped GaAs layer and the top gates on both ends of the beam form two piezoelectric capacitors, C_1 and C_2. A 15-nm-thick NiCr THz absorbing layer was deposited on the beam. This metal film was used also as a heater to calibrate the thermal responsivity of the resonator. The inset shows a blow-up of an SEM image of the hole array structure. (c) Schematic illustration for the measurement setup. An *ac* voltage was applied to one of the piezoelectric capacitors to drive the beam and the induced beam motion was monitored by a laser Doppler vibrometer. The motion signal is input to a phase locked loop (PLL) to provide a feedback control for maintaining the self-oscillation.

properties. Homogenous hole arrays of square lattices were formed on the GaAs MEMS beams. Owing to the reduction in the thermal conductance of the MEMS beams by introducing the hole array structures, the nano-porous samples shows 2-3 times larger thermal sensitivities than a reference unpatterned sample. Furthermore, because the heat capacitance of the MEMS beams is also reduced by the hole array structures, the thermal decay time of the nano-porous samples is increased only by about 30%~50%, demonstrating the effectiveness of the hole arrays for enhancing the thermal responsivities of bolometers without deteriorating their operation bandwidths significantly.

The wafer used for fabricating the doubly clamped MEMS beam resonators was grown by molecular beam epitaxy.[22] After growing a 200-nm-thick GaAs buffer layer and a 3-μm-thick $Al_{0.7}Ga_{0.3}As$ sacrificial layer on a (100)-oriented semi-insulating GaAs substrate, the beam layer was formed by depositing a 50-nm-thick GaAs layer, a GaAs/$Al_{0.3}Ga_{0.7}As$ superlattice structure, and a 400-nm-thick GaAs layer. We subsequently grew a 20-nm-thick Si-doped GaAs layer, a 70-nm-thick $Al_{0.3}Ga_{0.7}As$ layer and a 10-nm-thick GaAs capping layer. The fabrication process for the MEMS resonators with hole array structures were schematically shown in Fig. 1(a). The nanometer-scale hole array structures of the square lattice were patterned on the beam by using electron-beam lithography. The holes were formed by using reactive ion etching with Cl_2 gas and a rf power of 200 W at 50 °C for 80 s. The suspended beam structure was formed by selectively etching the sacrificial layer with diluted hydrofluoric acid.[22] Figure 1(b) shows an optical microscope image of a fabricated MEMS beam resonator (100×30×0.6 μm^3) with a 2D hole array structure of a hole diameter d = 500 nm and the neck size (the distance between neighboring holes) n = 500 nm. The inset of Fig. 1(b) shows a blow-up of an SEM image of the hole array structure, showing that the fabricated hole array is homogeneous. We fabricated MEMS beams with the hole array structures of various sizes, *i.e.*, d/n = 500 nm/500 nm, 500 nm/400 nm, 500 nm/300 nm, 300 nm/300 nm, and 300 nm/200 nm. In addition, we fabricated a reference sample without a hole array structure. The Si-doped GaAs layer and the top metal gates (15-nm-thick NiCr) on the two ends of the MEMS beam form two piezoelectric capacitors. An *ac* voltage was applied to one of the piezoelectric capacitors to drive the beam and the induced resonant beam motion was monitored by a laser Doppler vibrometer, as schematically shown in Fig. 1(c). The resonance signal is input to a phase locked loop (PLL) to provide a feedback control for maintaining a self-oscillation, as we reported elsewhere.[17] On the MEMS beam, we deposited a 15-nm-thick NiCr layer as a heater for calibrating the responsivity of the MEMS resonator, whose sheet resistance was ~500 Ω/□. All the measurements were performed in a vacuum (~10^{-4} torr) at room temperature.

Figure 2(a) shows the measured oscillation spectra of a MEMS resonator with a hole array structure (d/n = 300 2nm/200 nm) at various driving voltages (V_D = 10-80 mV) applied to the piezoelectric

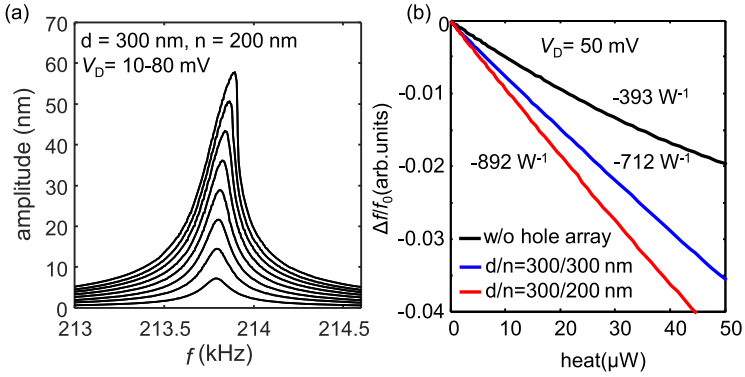

FIG. 2. (a) Resonance spectra of a MEMS beam resonator with a hole array structure (d/n = 300nm/200nm) measured by using an open-loop circuit (lock-in amplifier) at various driving voltages (V_D = 10-80 mV). (b) The normalized frequency shift ($\Delta f/f_0$) as a function of the input heating power, P_{in} = 0-50 μW, for two MEMS resonators with the hole array structures (d/n = 300nm/300nm and 300nm/200 nm) and that for a reference MEMS resonator. The numbers in the figure are the thermal responsivities $R \equiv \Delta f/f_0 P_{in}$ of these three samples determined from the slope of $\Delta f/f_0$.

© Author(s) 2019

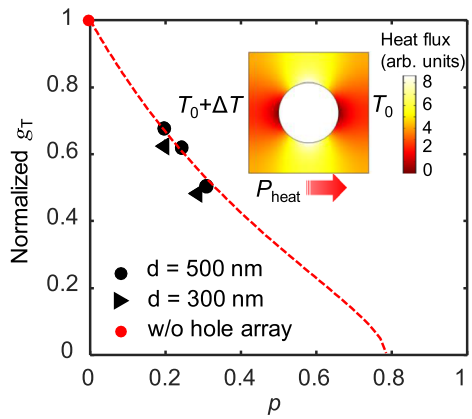

FIG. 3. Red dashed line plots the normalized thermal conductance of the unit cell of the square hole array lattice calculated as a function of the porosity of the nano-porous structure for a dimensionless unit cell (see the inset) by using finite element method. The symbols show the normalized thermal conductance of the nano-porous MEMS beams with various *d* and *n*, derived from the measured thermal decay time of the beams shown in Fig. 4(b), as a function of the porosity of the hole array structure.

capacitor. The resonance frequency, f_0, was about 213.8 kHz and the Q-factor was about 1,500. f_0 was higher than that of the reference MEMS resonator (~167.8 kHz). This is because the etching of the sacrificial layer develops through the holes for the nano-porous samples, whereas the etching proceeds only from the sides of the beam for the reference sample. This difference in the etching paths makes a difference in the length of the etching undercut, resulting in a shorter effective beam length for the nano-porous samples. When V_D exceeds 50 mV, the MEMS resonator shows a nonlinear hardening effect.

When an input power to the NiCr film, P_{in}, is increased from 0 to 50 μW, f_0 is reduced due to the thermal stress of the beam. Figure 2(b) shows the normalized frequency shift, $\Delta f/f_0$, as a function of the input heating power, P_{in}, for two MEMS resonators with hole array structures (d/n = 300 nm/300 nm and 300 nm/200 nm) and a reference MEMS resonator without the hole array. From the slope of the frequency shift shown in Fig. 2(b), we determined the thermal responsivity, $R \equiv \Delta f/(f_0 P_{in})$, for the samples. R is increased from ~393 W^{-1} for the reference sample to ~712 W^{-1} for d/n = 300 nm/300 nm and ~892 W^{-1} for d/n = 300 nm/200 nm, indicating that the hole array is effective in increasing the thermal responsivity of the MEMS detectors.

To back up our interpretation, we have calculated the thermal conductance of the unit cell of the square hole array lattice, g_T. Here, we introduce the porosity of the beam, p, which is defined by the ratio of the material volume removed from the beam to the volume of the beam before fabricating hole array structures,[19]

$$p = \frac{\pi d^2}{4(d+n)^2}. \tag{1}$$

As seen in Eq. (1), p is determined only by the ratio n/d. In the calculation, we assumed that the left and right boundaries of the hole array unit cell has a temperature difference, ΔT, and we calculated the heat power, P_{heat}, transmitted through the unit cell. g_T is defined as $g_T \equiv P_{heat}/\Delta T$. The red dashed line in Fig. 3 shows g_T as a function of the porosity of the hole arrays. The hole array structures fabricated in this work have a porosity of 0.2-0.3 and we expect that g_T is reduced by 40%~50% in our samples. In the figure, the inverse of the thermal responsivities of the hole array samples normalized by that of the unpatterned sample are also plotted. The measured inverse responsivities are in good agreement with the calculated g_T, indicating that the enhancement in R is indeed due to the reduction in G_T by introducing the hole arrays.

Next, to examine the effect of the hole array structures on the detection speed of the MEMS thermal sensors, we measured the thermal decay time, τ_D, of the beam by measuring the heat signal as a function of the modulation frequency, f_m. We drove the MEMS beam resonator in a self-oscillation mode by using a PLL and applied an ac voltage to the NiCr heater to generate a modulated heat of ~2.3 μW on the beam. From a simple thermal decay theory, the frequency shift, Δf, and the thermal decay time, τ_D, have a relationship expressed by;

$$\Delta f(f_m) = \frac{\Delta f_0}{\sqrt{1+(2\pi\tau_D f_m)^2}} G_{PLL}(f_m), \tag{2}$$

where Δf_0 is the frequency shift when the heat modulation frequency $f_m = 0$. $G_{PLL}(f_m)$ expresses the circuit response of the PLL.

We first characterized $G_{PLL}(f_m)$ to calibrate the effect of the demodulation bandwidth (BW) of the PLL. We input a frequency-modulated (FM) ac signal (amplitude = 1V, carrier frequency = 200 kHz, and FM depth 1 kHz) to the PLL to simulate the signal from the MEMS bolometer.[17] We swept f_m and measured the demodulated output of the PLL to obtain $G_{PLL}(f_m)$. Then,

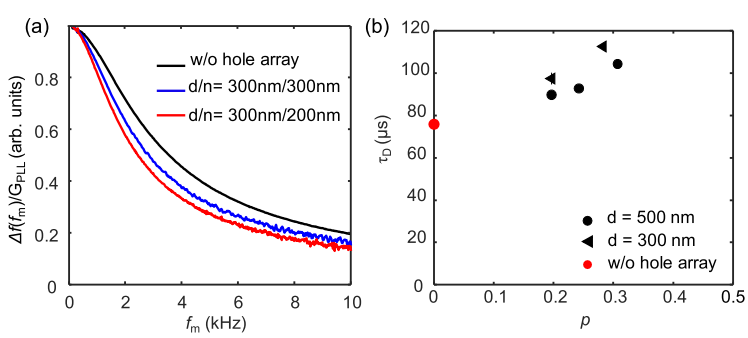

FIG. 4. (a) $\Delta f(f_m)/G_{PLL}$ measured for two nano-porous MEMS resonators (d/n=300nm/300nm and 300nm/200nm) and a reference sample. (b) Thermal decay time τ_D's of the beams with various hole array structures are plotted as a function of the porosity of the hole array structure. τ_D's were derived from the $\Delta f(f_m)/G_{PLL}$ spectra.

© Author(s) 2019

we can obtain the intrinsic frequency response of the beams as $\Delta f(f_m)/G_{PLL}(f_m)$, which is only determined by the thermal decay process in the MEMS beam. Figure 4(a) plots $\Delta f(f_m)/G_{PLL}(f_m)$ for a reference MEMS resonator without the hole array and two typical MEMS resonators with the hole array structures (d/n = 300 nm/300 nm and 300 nm/200 nm). As seen in the figure, the signals for the nano-porous samples decrease slightly faster than that of the reference sample, indicating that the thermal decay times, τ_D, are slightly increased by introducing the hole array structures.

By using numerical fitting of Eq. (2) to $\Delta f(f_m)/G_{PLL}(f_m)$, we obtained τ_D for the MEMS beams with the hole arrays and that for the reference MEMS beam. Figure 4(b) plots τ_D of the MEMS beams with the hole array structures as a function of p. τ_D is increased from ~75.8 μs for the reference sample to ~97.4 μs for d/n = 300 nm/300 nm and ~112.5 μs for d/n = 300 nm/200 nm. From Fig. 4(b), we see that the increase in τ_D by introducing the hole array structures is typically 30-50%. Compared with the improvement in responsivity (2-3 times), the reduction in the thermal BW is smaller, demonstrating effectiveness of the hole array structures for partly resolving the trade-off between the responsivity and the bandwidth of the thermal sensors.

Finally, we have characterized the noise equivalent power (NEP) of the MEMS beam resonators. We drove the MEMS beam resonators in a self-oscillation mode by using a PLL with a demodulation bandwidth of 1 kHz and measured the frequency noise spectra, n_f. Figure 5 plots n_f as a function of f_m for two MEMS resonators with hole arrays and a reference MEMS resonator. The samples with the hole arrays have slightly smaller frequency noise than the reference sample. Since the NEP of the MEMS resonator is expressed as NEP ≡ n_f/f_0R, the NEP is reduced by the enhanced thermal responsivities for the nano-porous samples. The minimum NEP for the reference sample was ~110 pW/Hz$^{0.5}$ at f_m = 1 kHz, whereas the NEP for the sample with d/n = 300 nm/300 nm is ~50 pW/Hz$^{0.5}$ and that for the sample with d/n = 300 nm/200 nm is ~40 pW/Hz$^{0.5}$. Since the detector sensitivity is defined by 1/NEP, the nano-porous MEMS resonators have 2-3 times larger sensitivities than the unpatterned reference sample.

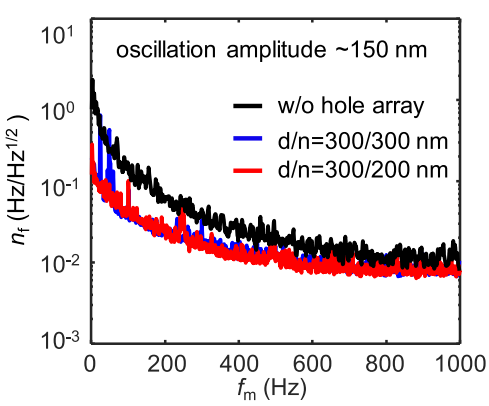

FIG. 5. Frequency noise spectra of the nano-porous MEMS resonators (d/n = 300nm/300nm and 300nm/200 nm) and the reference sample. The spectra were measured when the MEMS resonators were driven in a self-oscillation mode with a resonance amplitude of ~150 nm by a PLL with a modulation bandwidth of 1 kHz.

In summary, we have fabricated two-dimensional nanometer-scale hole array structures on GaAs doubly-clamped MEMS beam resonators to modulate their thermal properties. Owing to the reduction in the thermal conductance of the MEMS beams by introducing the hole array structures, the nano-porous samples with the hole array structures show 2-3 times larger thermal responsivities than an unpatterned reference sample. Furthermore, since the heat capacitance of the MEMS beams is also reduced by introducing the hole array structures, the thermal decay time of the nano-porous samples is increased only by about 30%~50%, demonstrating the effectiveness of the hole array structures for enhancing the thermal sensitivities of bolometers without deteriorating their operation bandwidths very much.

We thank Y. Watanabe for his contribution at the early stage of this work. This work has been supported by JST Collaborative Research Based on Industrial Demand (JPMJSK1514), KAKENHI from JSPS (17K14654), and MEXT Grant-in-Aid for Scientific Research on Innovative Areas "Science of hybrid quantum systems" (15H05868).

REFERENCES

[1] K. Ekinci and M. Roukes, Rev. Sci. Instrum. **76**, 061101 (2005).
[2] A. Boisen, S. Dohn, S. S. Keller, S. Schmid, and M. Tenje, Rep. Prog. Phys. **74**, 036101 (2011).
[3] A. N. Cleland, *Foundations of nanomechanics: from solid-state theory to device applications* (Springer Science & Business Media, 2013).
[4] K. L. Ekinci, X. M. H. Huang, and M. L. Roukes, Appl. Phys. Lett. **84**, 4469 (2004).
[5] S. Dohn, R. Sandberg, W. Svendsen, and A. Boisen, Appl. Phys. Lett. **86**, 233501 (2005).
[6] Y. T. Yang, C. Callegari, X. L. Feng, K. L. Ekinci, and M. L. Roukes, Nano Lett. **6**, 583 (2006).
[7] K. Jensen, K. Kim, and A. Zettl, Nat. Nanotech. **3**, 533 (2008).
[8] W. Pang, L. Yan, H. Zhang, H. Yu, E. S. Kim, and W. C. Tang, Appl. Phys. Lett. **88**, 243503 (2006).
[9] A. N. Cleland and M. L. Roukes, Nature **392**, 160 (1998).
[10] R. Knobel, C. S. Yung, and A. N. Cleland, Appl. Phys. Lett. **81**, 532 (2002).
[11] S. C. Masmanidis, H. X. Tang, E. B. Myers, M. Li, K. De Greve, G. Vermeulen, W. Van Roy, and M. L. Roukes, Phys. Rev. Lett. **95**, 187206 (2005).
[12] K. Onomitsu, I. Mahboob, H. Okamoto, Y. Krockenberger, and H. Yamaguchi, Phys. Rev. B **87**, 060410 (2013).
[13] A. K. Pandey, O. Gottlieb, O. Shtempluck, and E. Buks, Appl. Phys. Lett. **96**, 203105 (2010).
[14] T. Larsen, S. Schmid, L. Grönberg, A. Niskanen, J. Hassel, S. Dohn, and A. Boisen, Appl. Phys. Lett. **98**, 121901 (2011).
[15] Y. Zhang, Y. Watanabe, S. Hosono, N. Nagai, and K. Hirakawa, Appl. Phys. Lett. **108**, 163503 (2016).
[16] Y. Zhang, S. Hosono, N. Nagai, and K. Hirakawa, Appl. Phys. Lett. **111**, 023504 (2017).
[17] Y. Zhang, S. Hosono, N. Nagai, S.-H. Song, and K. Hirakawa, J. Appl. Phys. **125**, 151602 (2019).
[18] R. Yanagisawa, J. Maire, A. Ramiere, R. Anufriev, and M. Nomura, Appl. Phys. Lett. **110**, 133108 (2017).
[19] D. Song and G. Chen, Appl. Phys. Lett. **84**, 687 (2004).
[20] J. Maire, R. Anufriev, R. Yanagisawa, A. Ramiere, S. Volz, and M. Nomura, Science Advances **3**, e1700027 (2017).
[21] M. Nomura, J. Shiomi, T. Shiga, and R. Anufriev, Jpn. J. Appl. Phys. **57**, 080101 (2018).
[22] I. Mahboob and H. Yamaguchi, Nat. Nanotech. **3**, 275 (2008).

© Author(s) 2019